Optical layout for a 10 m Fabry–Perot Michelson interferometer with tunable stability

2012 Class. Quantum Grav. 29 075003

(http://iopscience.iop.org/0264-9381/29/7/075003)

Class. Quantum Grav. **29** (2012) 075003 (13pp) doi:10.1088/0264-9381/29/7/075003

Optical layout for a 10 m Fabry–Perot Michelson interferometer with tunable stability

Christian Gräf[1], Stefan Hild[2], Harald Lück[1], Benno Willke[1], Kenneth A Strain[2], Stefan Goßler[1] and Karsten Danzmann[1]

[1] Max-Planck-Institut für Gravitationsphysik (Albert-Einstein-Institut) and Leibniz Universität Hannover, Callinstr. 38, D-30167 Hannover, Germany
[2] SUPA, School of Physics and Astronomy, The University of Glasgow, Glasgow G12 8QQ, UK

E-mail: christian.graef@aei.mpg.de

Received 8 December 2011, in final form 2 February 2012
Published 14 March 2012
Online at stacks.iop.org/CQG/29/075003

Abstract
The sensitivity of high-precision interferometric measurements can be limited by Brownian noise within dielectric mirror coatings. This occurs, for instance, in the optical resonators of gravitational wave detectors where the noise can be reduced by increasing the laser beam size. However, the stability of the resonator and its optical performance often impose a limit on the maximally feasible beam size. In this paper, we describe the optical design of a 10 m Fabry–Perot Michelson interferometer with tunable stability. Our design will allow us to carry out initial commissioning with arm cavities of high stability, while afterward the arm cavity length can be increased stepwise toward the final, marginally stable configuration. Requiring only minimal hardware changes, with respect to a comparable 'static' layout, the proposed technique will not only enable us to explore the stability limits of an optical resonator with realistic mirrors exhibiting inevitable surface imperfections, but also the opportunity to measure coating Brownian noise at frequencies as low as a few hundred hertz. A detailed optical design of the tunable interferometer is presented and requirements for the optical elements are derived from robustness evaluations.

PACS numbers: 04.80.Nn, 07.60.Ly, 42.50.Lc

(Some figures may appear in colour only in the online journal)

1. Introduction

The AEI 10 m Prototype [1, 2] is an ultralow displacement noise facility, incorporating a large ultrahigh vacuum system, excellent seismic isolation and a well-stabilized high-power laser source, and is intended to host a variety of interferometry experiments. One of these experiments is planned to be a Fabry–Perot Michelson interferometer which is intended to

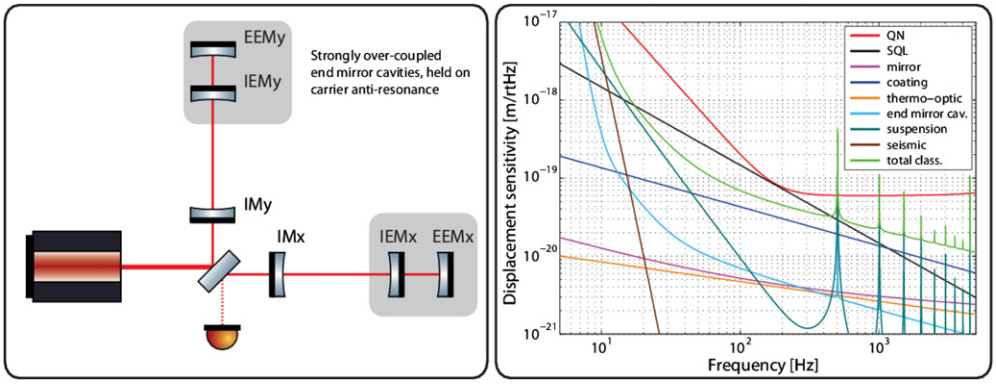

Figure 1. Left: schematic drawing of the AEI 10 m sub-SQL interferometer target configuration, as presented in [3]. Topology-wise the interferometer is planned to be a Fabry–Perot Michelson interferometer with an arm length of approximately 10 m. For the reduction of coating Brownian thermal noise, it is intended to replace the conventional highly reflective arm cavity end mirrors with short, strongly overcoupled cavities which will be held on anti-resonance for the carrier light by means of feedback control. Right: anticipated noise spectral densities of components of the expected measurement noise for the target configuration. The total classical noise curve is the quadrature sum of residual seismic noise together with several thermal noise components: internal thermal noise (mirror), coating noise, thermo-optic noise and suspension thermal noise. An additional contribution to the total classical noise, specific to this design, stems from end mirror cavity-induced phase noise, cf [4]. In the most sensitive frequency band, the total classical noise is below the sum of quantum radiation pressure and shot noise, thereby enabling a purely quantum noise-limited measurement of the differential interferometer arm length.

operate at a purely quantum noise-limited sensitivity in its detection band at hundreds of hertz [3]. At a frequency of approximately 200 Hz, this instrument will be capable of reaching the standard quantum limit (SQL) of optical interferometry for 100 g mirrors.

A schematic drawing of the original interferometer conceptual design configuration, which in the following we will refer to as the 'target configuration', is shown in figure 1, along with the anticipated noise spectral densities.

It is evident that in the design of an instrument to reach the SQL, quantum noise must dominate over the sum of classical contributions which must be minimized. As in the case of large-scale advanced gravitational wave (GW) detectors, coating Brownian thermal noise is identified to be the most prominent classical noise source in the noise budget of the AEI 10 m sub-SQL interferometer.

This paper reports on a stepwise approach to reducing coating thermal noise by iteratively enlarging the beam spots on the interferometer's arm cavity optics toward the technically feasible maximum. This goes hand in hand with pushing the arm cavities toward their geometric stability boundary.

The use of extremely large laser beam spots is a key feature in the target configuration of the AEI 10 m sub-SQL interferometer to reduce coating thermal noise below quantum noise level, which is motivated by the theoretical model for coating thermal noise given in [5]. This instrument is planned to be operated with beam spots with an equal radius of $w \approx 9.7$ mm on all cavity mirrors, which have a radius of $a = 24.3$ mm. In this sense, we regard our proposed setup as an intermediate, simplified configuration to pave the way to eventually building and operating our target configuration described in [3].

Table 1. Comparison of arm cavity lengths and radii of curvature of cavity mirrors and the resulting cavity *g*-factors for large-scale second- and third-generation GW observatories and the planned AEI 10 m sub-SQL interferometer. Whereas second-generation observatories exhibit a generous safety margin in their cavity stabilities, which is planned to be considerably smaller in the third-generation detectors, the AEI sub-SQL interferometer arm cavities will eventually be operated extremely close to the stability boundary.

		Radius of curvature		
	Cavity length	Input mirror	End mirror	Cavity *g*-factor
Advanced LIGO [8]	3996 m	1934 m	2245 m	0.832
Advanced Virgo [9]	3000 m	1420 m	1683 m	0.871
ET-B [10]	10 000 m	5070 m	5070 m	0.945
Sub-SQL IFO simplified design:				
Initial configuration	10.8 m	5.7 m	5.7 m	0.8
Marginally stable configuration	11.3952 m	5.7 m	5.7 m	0.998

2. Challenges of stably operating the target configuration

The attempt to operate a Fabry–Perot Michelson interferometer with extremely large beam spots on the cavity mirrors inevitably comes at the expense of poor resonator stability. The notion of stability of an optical resonator is closely connected to the existence of low-loss cavity eigenmodes. With the aid of the formalism introduced in [6], we can quantify the stability of an optical resonator as a function of the mirrors' radii of curvature and their spatial separation. This measure is commonly referred to as the cavities' *g-factor*.

In marginally stable (i.e. $g \simeq 1$) optical resonators, even small-scale length perturbations or mirror curvature error can render the instrument unstable. Implications of this are e.g. a dramatic increase of optical losses and a deterioration of heterodyne signals [7], which are extracted for interferometer feedback control. As a consequence, poor stability may prevent the instrument from reaching its sensitivity goal and may severely impede its operability, respectively.

2.1. Typical stabilities of the target configuration

Our laboratory environment, basically the vacuum system, imposes space constraints on the minimum and maximum arm length of our interferometer. In this respect, for the target configuration shown in figure 1, typical arm cavity lengths are of the order $L_{\mathrm{arm}} \approx 10.4\,\mathrm{m}$. Another boundary condition with an impact on cavity lengths and mirror radii of curvature is the requirement for beam spots with a designated radius of $w = 9.7$ mm, which stems from a trade-off between low coating thermal noise and diffraction loss. Obeying these boundary conditions, calculations yield an arm cavity *g*-factor of typically $g = 0.999$[3]. For such a configuration, a cavity length or a radius of curvature (RoC) error of only a few mm would be sufficient to render the cavity unstable.

For the purpose of comparison, typical arm cavity stabilities of large-scale interferometric GW detectors and the AEI 10 m sub-SQL interferometer are summarized in table 1.

[3] It must be noted that all stability estimates are approximate in the sense that they are based on the assumption of perfectly spherical optics. For more meaningful predictions of the stability, realistically imperfect optics need to be taken into account. In the experiment, we propose to obtain surface maps of the actual mirrors, and to simulate the effect on stability. This is beyond the scope of this paper.

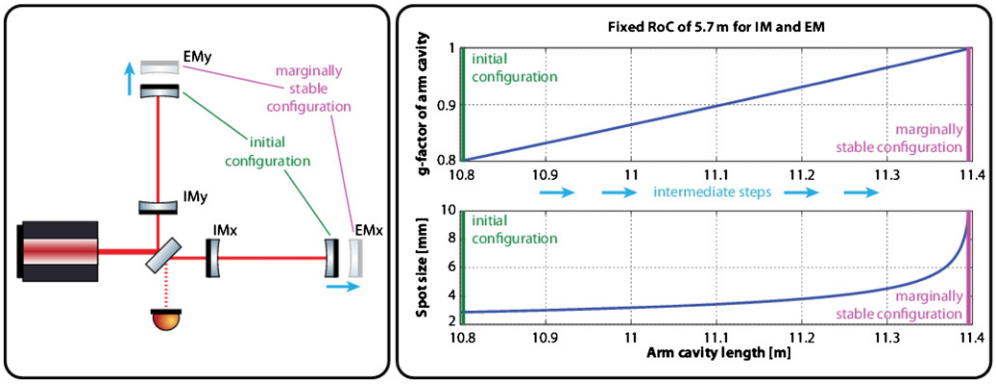

Figure 2. Beam size and g-factor of a symmetric arm cavity of variable length with input mirror and end mirror curvature of the HR (high reflective-coated) surfaces of $R_{\mathrm{IM}}^{\mathrm{HR}} = R_{\mathrm{EM}}^{\mathrm{HR}} = 5.7$ m. The right end of the plot characterizes the marginally stable configuration of the AEI 10 m sub-SQL interferometer which features extremely large beam spots and a g-factor close to instability. However, using exactly the same mirrors, but an arm cavity length shortened to $L_{\mathrm{arm}} = 10.8$ m, we can reduce the g-factor to a comfortable value of $g = 0.8$ while reducing the beam size of $w = 9.72$ mm to $w = 2.86$ mm.

3. Motivation for a stepwise approach toward the final beam size

In this paper, we propose a *stepwise approach toward the final beam size* in order to ease the commissioning of the AEI 10 m sub-SQL interferometer. This approach will allow us to initially learn how to operate the interferometer with relatively small beam spots on the cavity optics and therefore more comfortable arm cavity stability. After having established stable operation in the initial configuration and gathering the required experience, we can then approach the marginally stable configuration by iteratively enlarging the beam size on the main mirrors toward its design value.

For this stepwise approach to be feasible, it is crucial to find a way of increasing the beam size that does not require any major hardware changes, such as for instance replacing main optics. It would for example be impractical and too cost intensive to adjust the beam size in the arm cavities by swapping the main mirrors with the ones with a different RoC, especially as the mirrors feature monolithic suspension systems. Systems to thermally actuate on mirror curvatures have been successfully demonstrated [11, 12] but provide an insufficient actuation range for our application[4].

However, as the AEI Prototype infrastructure provides sufficient space to shift the positions of the main mirrors by up to about 1 m or 10% of the arm cavity length, we have the possibility of reducing the beam size on the optics without adjusting the main mirror RoC, but by initially shortening the arm cavity length. Let us assume design values for the arm cavity length of $L_{\mathrm{arm}} = 11.395$ m and radii of curvature of the input mirrors' (IM) and end mirrors' (EM) high reflective-coated (HR) surfaces of $R_{\mathrm{IM}}^{\mathrm{HR}} = R_{\mathrm{EM}}^{\mathrm{HR}} = 5.7$ m. Such an arm cavity would have a g-factor of $g \approx 0.998$. As shown in figure 2, we can achieve a comfortable g-factor of $g = 0.8$ with exactly the same mirrors by just shortening the distance between the input and end mirror by about 0.6 m to a total arm cavity length of $L_{\mathrm{arm}} = 10.8$ m. Such a shortening of the arm

[4] A tuning range of the cavity g-factor similar to our proposed approach would require to change the sagitta of our arm cavity mirrors in the order of microns. To achieve this, our mirrors would have to be heated by hundreds of kelvins.

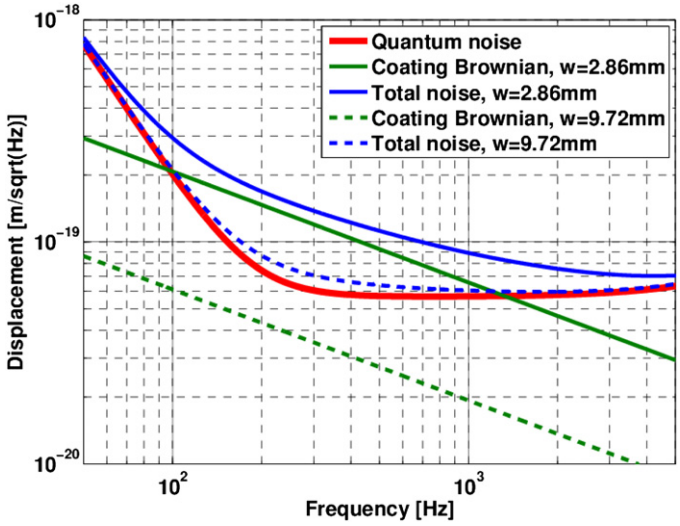

Figure 3. Simplified displacement sensitivity graph for the AEI 10 m sub-SQL interferometer only including the quantum noise and coating Brownian noise contributions for the initial configuration of 10.8 m arm cavity length (solid traces) and the marginally stable configuration (dashed traces) with $L_{\mathrm{arm}} = 11.395$ m arm cavity length. The quantum noise (red) is independent of the arm cavity length. With the initial configuration, we expect to be able to directly measure the coating Brownian noise in the frequency range between 100 Hz and 1 kHz, while in the marginally stable configuration with large beam spots thermal noise contributions will be significantly below the quantum noise.

cavity length corresponds to reducing the beam size on the main mirrors from the targeted value of $w = 9.72$ mm to an initial beam size of only $w = 2.86$ mm (see the lower-right subplot of figure 2).

3.1. Direct measurement of coating Brownian noise

Starting with the $L_{\mathrm{arm}} = 10.8$ m configuration will not only be advantageous for commissioning of the interferometer and noise hunting, but will also allow us to directly measure coating Brownian noise. Figure 3 shows the fundamental noise limits of the simplified AEI 10 m sub-SQL interferometer design for the marginally stable configuration with $L_{\mathrm{arm}} = 11.395$ m arm length and the initial configuration with $L_{\mathrm{arm}} = 10.8$ m long arm cavities. Since the beam size on all main mirrors is different by about a factor 3.5 between the two arm cavity lengths, the coating Brownian noise will scale accordingly, thus offering us the possibility of directly measuring coating Brownian noise at frequencies between about 100 Hz and 1 kHz with the initial configuration. This is an interesting opportunity to verify the coating Brownian noise level at frequencies around 200 Hz, which is the frequency range where coating Brownian noise is most important for the advanced GW detectors, and which has so far not been accessible by direct measurement [13, 14].

3.2. Potential impact on future GW detectors

One of the major steps for improving the sensitivity from the first- to second-generation GW detectors was to significantly increase the beam size on the main test masses, especially at the

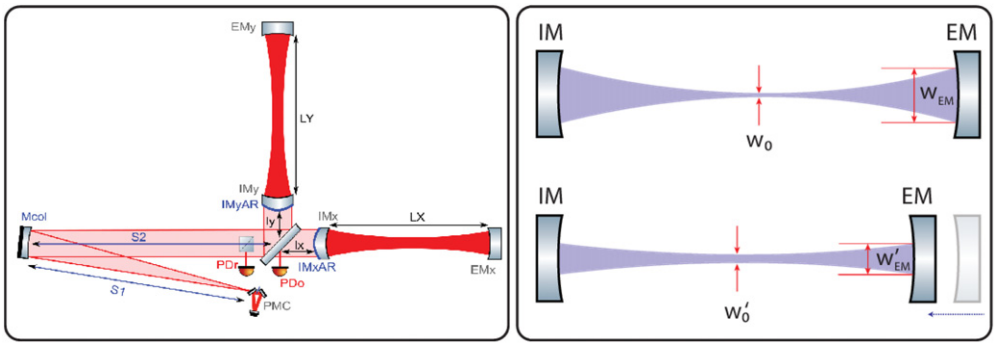

Figure 4. Left: simplified schematic drawing of the building blocks of the tunable cavity length configuration. The beam with a waist defined by the triangular pre-mode cleaner cavity (PMC) propagates to a curved collimating mirror at a distance of about 12 m. The reflected beam is directed into the interferometer where it is matched to the arm cavities' fundamental eigenmodes by means of curved arm cavity input mirror AR surfaces. Right: moving the arm cavities' end mirrors alters the fundamental arm cavity eigenmode. For our starting configuration, which features shorter arm cavities than the marginally stable design configuration, we find a larger beam waist at a shorter distance from the input mirror as well as smaller beam spots on both cavity mirrors.

input mirrors. If larger mirror substrates become available, future upgrades to these advanced detectors might include even further increased beam sizes on the mirrors in order to reduce the influence of thermal noise contributions. This would require to operate the arm cavities with g-factors even higher than the ones stated in table 1.

The experience we will gain from the AEI 10 m sub-SQL interferometer by step-wise approaching the cavity g-factor of $g = 0.998$ will allow us to study destabilizing effects and stability limitations for related experiments. These results combined with reliable simulations can be at least partially transferred to upgrades of second-generation GW detectors as well as to third-generation GW detectors and may provide guidance in determining maximally feasible beam sizes for these instruments.

4. Properties of the optical configuration with tunable stability

Unlike the typical scenario in which Fabry–Perot Michelson interferometers are applied, in which the arm cavity geometry is not changed during the lifetime of the experiment, the primary goal for the AEI 10 m sub-SQL interferometer optical design is to identify a configuration which fulfills the requirement of tunable arm cavity stability or, synonymously, which can be operated equally well for different beam spot sizes on the cavity mirrors (cf section 3).

Owing to the fact that each iteration step, at discrete arm cavity lengths, will feature distinct cavity eigenmodes, it follows that the implementation of a flexible mode-matching scheme is the most elegant approach to solving this problem. The performance goals of the instrument require close to optimal mode matching of the cavities at all times.

The starting point for our proposed optical configuration is the generation of a collimated laser beam with tunable radius. This forms the input beam to the interferometer and is matched into the arm cavity eigenmodes by curved rear (antireflection coated) surfaces on the substrates of the input mirrors. A schematic drawing of this concept is depicted in the left pane of figure 4.

4.1. Collimated interferometer input beam

From the technical point of view, a collimated beam can easily be prepared by including a curved mirror into the input optics chain and by choosing the mirror's RoC and its distance to the input beam waist appropriately. To minimize the astigmatism introduced by the collimating mirror, the opening angle between the incident and the reflected beam should be as small as possible. This can be achieved by increasing the distance of beam propagation of the incoming and outgoing beam, e.g. by positioning the collimating mirror near one of the interferometer arm cavity end mirrors.

Using a collimated input beam has a number of advantages over using a diverging beam[5]. It is generally desired to have a high level of symmetry of the interferometer arms because this has a high impact on the intrinsic cancellation of common mode perturbations at the beam splitter. On the other hand, to provide transmission of RF control sidebands to the detection port of the interferometer, which is typically locked on or very close to a dark fringe, it is necessary to introduce a macroscopic offset in the path lengths between the two arm cavity input mirrors and the beam splitter. This offset is referred to as the *Schnupp asymmetry* [15]. For a non-collimated input beam, the propagation over unequal path lengths would lead to beam parameters which were different on the parallel and the perpendicular arm cavity IMs. If perfect mode matching were to be achieved for both arm cavities, this configuration would require either to include additional optics or to have different radii of curvatures for the AR surfaces on the input mirrors.

A further benefit of using a collimated input beam is the reduction of astigmatism introduced at the beam splitter.

4.2. Coupling efficiency of the flexible mode-matching scheme

A natural measure to benchmark our proposed layout, especially with respect to the flexibility of the mode-matching scheme, is the theoretical mode coupling efficiency for the extreme cases, i.e. the initial configuration and the marginally stable configuration. The mode-matching efficiency η,

$$\eta = \frac{\left| \iint \mathrm{d}x\,\mathrm{d}y\, \Psi(x,y,z)\, \hat{\Phi}^*(x,y,z) \right|^2}{\iint \mathrm{d}x\,\mathrm{d}y |\Psi(x,y,z)|^2 \times \iint \mathrm{d}x\,\mathrm{d}y |\hat{\Phi}(x,y,z)|^2}, \tag{1}$$

which is referred to several times throughout this paper, is a measure of the coupling of optical power into a fundamental cavity eigenmode. It is defined as the normalized overlap integral of the TEM_{00} mode of the laser beam Ψ and the fundamental cavity eigenmode $\hat{\Phi}$. The modes Ψ and $\hat{\Phi}$ are fully determined by the complex beam parameters $q(z)$ and $\hat{q}(z)$ of the input beam and eigenmode at an arbitrary position $z = z_0$ along the beam axis of propagation.

The calculated efficiency can be regarded as an upper bound to the practically achievable mode-matching quality.

We consider the marginally stable configuration as the reference, meaning that in our analysis all relevant parameters are chosen with respect to achieving perfect mode matching for this configuration. By keeping all parameters, except for the arm cavity length, constant, we can quantify the degradation of the mode matching and identify possibilities for the recovery of the mode matching as well as limits to the degree by which it is recoverable.

In our case, the mode-matching efficiency is determined by two parameters: the radius of the collimated input beam and the RoC of the arm cavity input mirrors' AR surfaces. For the

[5] A possible downside may be a potentially higher susceptibility to beam pointing noise. A detailed analysis of this effect is, however, not within the scope of this paper.

marginally stable configuration with an arm cavity length of $L_{\mathrm{arm}} = 11.3952$ m and mirror high reflectivity (HR) surface radii of curvature of $R_{\mathrm{IM}}^{\mathrm{HR}} = R_{\mathrm{EM}}^{\mathrm{HR}} = 5.7$ m, we find an input beam radius of $w \approx 9.74$ mm and an IM AR surface RoC of $R_{\mathrm{IM}}^{\mathrm{AR}} \approx 1.776$ m to result in a perfect mode matching to the arm cavities.

Ideally, in the real interferometer, the arm cavity length is changed in each iteration step by moving the end mirrors only; this we adopt as a further boundary condition for the stepwise cavity length tuning. If we now keep the optimal values of the marginally stable configuration for all parameters, except for the arm cavity length which we reduce to a value of $L_{\mathrm{arm}} = 10.8$ m by shifting the end mirror toward the input mirror, we observe a substantial decrease of the mode-matching efficiency. This scenario corresponds to setting up the initial configuration with improved stability with optics that are optimized for marginally stable operation.

Owing to the fact that the RoC of the IM AR surfaces cannot be easily changed in practice, this value is to be considered a constant for all length iteration steps. On the contrary, the radius of the collimated input beam can be tuned to recover the beam matching to the cavities' eigenmodes. According to this, by tuning the radius of the collimated input beam down to $w \approx 2.88$ mm, the matching efficiency for the configuration with shortened arms can be $\eta > 99\%$, albeit the limitation of the radius of the collimated input beam being the only parameter available for optimization. Aspects of the technical realization of a tunable collimated input beam are addressed in section 4.3.

Based on experience gained from earlier experiments, we consider a degradation of the mode-matching efficiency of not more than 1% (with respect to the perfectly matched case) tolerable in the sense that this is likely to have a negligible impact on the performance of the instrument. A more elaborate estimation of this requirement based on a detailed noise analysis is subject to future work.

The mode-matching efficiency as a function of the radius of the collimated input beam and the RoC of the arm cavity input mirror AR surfaces for the two arm cavity length extremes is shown in figure 5.

The residual degradation in the short arm cavity case can be attributed to a waist position mismatch within the cavities, which cannot be compensated by tuning the input beam radius. This is due to the fact that the focal distance of the curved IM AR surface for the collimated input beam is constant, whereas the position of the waist of the arm cavity eigenmode is a function of the cavity length. Due to the symmetry of the configuration, the waist position moves toward the IMs by half the length change. This is illustrated in the right pane of figure 4. The evolution of the mode-matching efficiency as a function of the collimated input beam radius and the arm cavity length is shown in figure 6.

4.3. Further operational requirements

In our case, besides the introduction of the curved collimating mirror, the input optics chain needs to be extended by optics to implement the required feature of radius tunability of the collimated beam. The notion of *input optics* commonly summarizes the optical elements which serve the purpose to deliver a pure, well-aligned beam with the optimal geometry to the interferometer[6].

It is possible to conceive various approaches to implementing adjustable mode matching in the input chain. Obvious examples include exchanging the collimating mirror in each iteration step and introducing a beam expanding telescope in the collimated beam path, but these turn out to be poor choices. Whereas the former option depends on the time-consuming

[6] For conciseness, further optical elements such as electro-optic modulators, isolators, etc, which are usually required elements of the input optics chain, are omitted in this discussion.

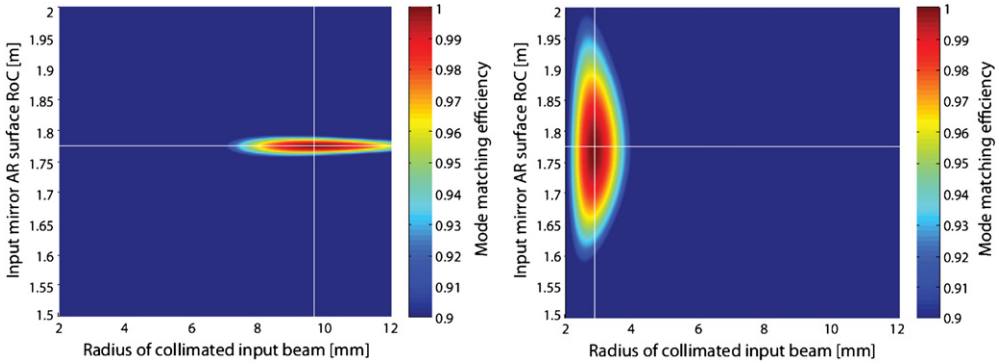

Figure 5. Mode-matching efficiency maps of the interferometer arm cavities. The left plot corresponds to the marginally stable configuration with an arm cavity length of $L_{\mathrm{arm}} = 11.395$ m, and the plot on the right-hand side illustrates the situation for the starting configuration with a reduced arm cavity length of $L_{\mathrm{arm}} = 10.8$ m. In both maps, the mode-matching efficiency is color coded as a function of the radius of the collimated interferometer input beam and the RoC of the AR surface of the arm cavity input mirrors. By holding the IM AR surface RoC constant and changing the input beam radius, only a mode-matching efficiency for the short arm cavity configuration can be obtained which is degraded by approximately 1% of the (theoretically perfect) matching efficiency of the marginally stable configuration. All numerical investigations were carried out by means of the matrix formalism introduced in [6] as well as the interferometer simulation software *Finesse* [16].

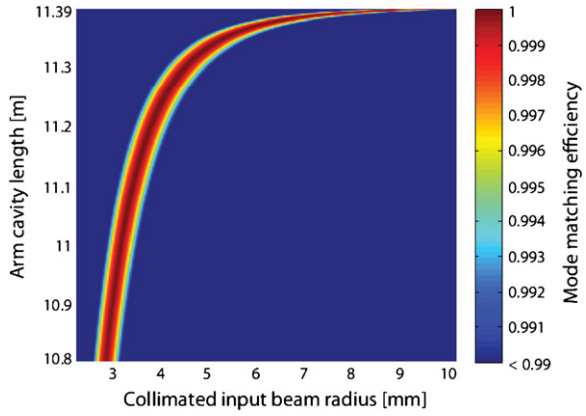

Figure 6. Mode-matching efficiency of the interferometer arm in the reflected port of the beam splitter (with respect to the input beam) as a function of the radius of the collimated input beam and the arm cavity length. For the RoC of the arm cavity input mirror AR surface, a value of $R_{\mathrm{IM}}^{\mathrm{AR}} = 1.776$ m was implicitly assumed. Whereas in theory perfect mode matching can be achieved for the marginally stable design configuration, a mode-matching efficiency of up to 99% is theoretically feasible for the starting configuration with shorter arm cavities.

task of replacing a suspended optic and gives rise to a complicated realignment procedure in each iteration step, the latter, likewise, requires frequent swapping of optics and may furthermore be an additional source of optical aberrations.

Our preferred method of input beam shaping is to tune the waist radius of the *initial* beam, while keeping the waist position constant, prior to its reflection at the collimating mirror. This

can, for instance, be accomplished by means of a beam telescope in combination with a beam expander, which consists of lenses or mirrors. These can easily be shifted on the optical table for fine tuning. The use of active optics may help to avoid the need to exchange fixed focal length optical elements.

A matter closely related to the stable operation of the tunable length interferometer is the sub-area of sensing and control of the optical degrees of freedom of the instrument. Typically, RF modulation-based heterodyne length signal extraction schemes are employed, which require one or more electronic local oscillators as signal sources, whose frequencies are optimized with respect to cavity lengths within the interferometer to be controlled [17]. In our case, the cavity length tunability may require a flexible RF modulation scheme.

However, a detailed treatment of this topic, which can be regarded as a technical issue, rather than fundamental, is beyond the scope of this paper and shall be discussed elsewhere.

5. Estimation of the operational robustness

Parameters in the optical layout may deviate from their designated values for a variety of reasons, e.g. fabrication tolerances, environment-induced drifts or the nature of the experimental apparatus itself. Ideally, the interferometer design should exhibit a high level of immunity to tolerances in its constituting parameters. Practically, we find imperfections in the optical elements and inaccuracies in the optical setup to degrade the performance of the interferometer or, in the worst case, to even render the instrument inoperable.

On the basis of the schematic shown in figure 4, we can identify design parameters which have a direct impact on the maximally achievable mode-matching efficiency. These are the initial beam waist radius w_0 as well as its position z_0 (defined by the eigenmode of the triangular cavity in figure 4), the RoC of the collimating mirror as well as its position on the table and the RoC of the IMs' AR surfaces.

In this section, we investigate the impact of deviations of these parameters from their design values. This knowledge can in turn be utilized to formulate specifications for the required manufacturing precision for the optics.

5.1. Initial laser beam waist radius and position

Provision of an initial beam with well-defined beam parameters is crucial to meet the requirement for a well-collimated interferometer input beam with a specific radius for each cavity length iteration step. A mismatch of the actual parameters of the initial beam with respect to the ideal ones is likely to have a direct impact on the mode-matching quality.

The dependence of the arm cavity mode-matching efficiency on the initial beam waist position z_0 is depicted in the top-left plot in figure 7. Clearly, a deviation of the waist position along the optical axis can be compensated by shifting the position of the collimating mirror by the same amount.

It is noteworthy that shifting the collimating mirror position simultaneously alters the length of the incoming as well as the outgoing beam path. Nevertheless, due to the reflected beam being collimated, this coupling of the two lengths is neutralized in first order. Consequently, the quality of the mode matching is mostly insensitive to length changes in this path.

Small deviations of the initial beam waist radius from the optimum can be found to have a negligible effect on the mode coupling efficiency, cf bottom-left plot in figure 7. A deviation of $\pm 5\%$ in w_0 results in a degradation of the mode-matching efficiency of less than 0.5%.

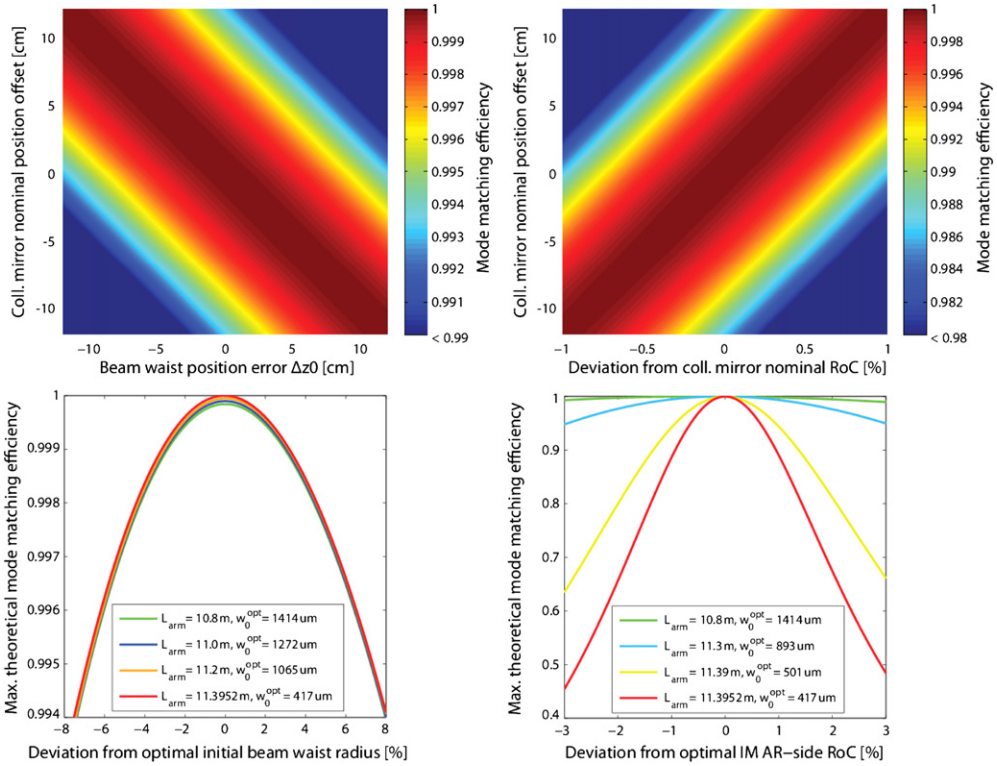

Figure 7. Degradation of the theoretically achievable mode-matching efficiency due to deviations of design parameters from their respective optima. Top left: a mismatch in the input beam waist position z_0 can be compensated by shifting the position of the collimating mirror on the table. Top right: likewise, imperfections of the collimating mirror RoC can be compensated by shifting the mirror's position. Bottom left: the mode-matching efficiency exhibits fairly low susceptibility to deviations from the optimal initial beam waist radius w_0. A deviation of $\pm 5\%$ in w_0 results in a mode-matching efficiency degradation of less than 0.5%. Note that none of the configurations, except for the marginally stable one, reaches perfect mode matching. Bottom right: the susceptibility to IM AR surface RoC error increases with the arm cavity length approaching the marginally stable case. In the marginally stable configuration, a deviation of $\pm 1\,\%$ comes at the expense of a mode-matching efficiency degradation of $\approx 11.2\,\%$.

5.2. Collimating mirror RoC imperfections

The effect of RoC imperfections of the collimating mirror as well as a possible workaround is illustrated in the top-right plot in figure 7.

A RoC error results in a non-optimal focal length of the mirror. The focal length, in turn, is required to match the distance to the initial beam waist to perfectly collimate the beam in reflection. Again, the collimating mirror position can be shifted to compensate this type of imperfection. The same argument of length offsets in the reflected beam path being negligible (see the previous section) holds here, too. Alternatively, instead of shifting the mirror position, the RoC could e.g. be thermally actuated upon.

5.3. Input mirror AR surface RoC

The susceptibility of the mode-matching efficiency to RoC imperfections of the IMs' AR surfaces is illustrated in the lower-right plot in figure 7. It becomes evident that whereas for the

starting setup the arm cavity mode matching shows comparatively low susceptibility to this type of imperfection, the effect increases as we approach the marginally stable configuration arm cavity length. While for the initial configuration it takes a RoC error of $\pm 3.2\%$ to degrade the mode matching by $\approx 1\%$, for the marginally stable setup, we find a RoC deviation of $\pm 1\,\%$ to result in a mode-matching efficiency degradation of $\approx 11.2\%$. A mode-matching efficiency of $\eta \gtrsim 99\%$ for all configurations, including the marginally stable one, could be achieved by means of an IM AR surface RoC error lower than $\pm 0.28\%$, which corresponds to an absolute RoC error of ± 5 mm.

Unlike the cases discussed previously, for the IM AR surface RoC there is no well-decoupled degree of freedom in the instrument available that can be utilized to easily compensate an error in this parameter. Direct thermal actuation does not pose a suitable solution as the radii of curvature on both sides of the mirror would be affected simultaneously, leading to an unwanted distortion of the cavity eigenmode. However, depending on its nature, a residual RoC error in both IM AR surfaces could be tackled by different means.

A 'common mode' RoC error (i.e. the sign of both RoC deviations, for the parallel and the perpendicular interferometer arm IM, is identical) of both IMs could be compensated by slightly tuning the divergence angle of the interferometer input beam. This could be achieved by means of shifting the collimating mirror from its optimal position or actuating on its RoC (e.g. thermally). The pivotal point of this approach is to trade waist radius error for waist position error, the latter of which the cavity mode-matching efficiency is generally less susceptible to. If, for instance, in the marginally stable configuration the actual IM AR surface RoC turns out to be smaller by 1% with respect to its optimal value of $R_{\mathrm{IM}}^{\mathrm{AR}} = 1.776$ m, the mode-matching efficiency can be recovered to $\eta \gtrsim 99\%$ by increasing the RoC of the collimating mirror. For typical beam path lengths in the collimating stage, the required change of the collimating mirror RoC would be of the order of tens of centimeters. Alternatively, the same can be achieved by shifting the initial beam waist out of the focal point of the collimating mirror, with an offset of the same order as the previously described collimating mirror RoC change.

A 'differential' RoC error is in general harder to handle but could, if absolutely necessary, be compensated by introducing additional optical elements in the central Michelson arms, i.e. between the beam splitter and the arm cavity IMs.

As mentioned previously, first and foremost these compensation techniques are relevant for configurations very close or at the marginally stable arm cavity length, only if mirror AR surface RoC fabrication errors turn out to be larger than desired. For the larger part of the operation modes, in terms of different cavity lengths, no such measures need to be taken.

6. Summary and outlook

In this paper, we have described a detailed optical layout for the AEI 10 m sub-SQL interferometer based on a robust procedure to bring the interferometer to its final configuration with marginally stable arm cavities. Starting with the arm cavities set to be shorter than eventually required, but with all other parameters unchanged, significantly increased stability of the arm cavity eigenmode may be obtained. This is desirable to allow initial commissioning of the AEI 10 m sub-SQL interferometer. A step-by-step approach to the final cavity mode is proposed.

In order to realize a close-to-optimal mode matching to the arm cavities, over the whole range of spot sizes, we employ a collimated beam of variable size in combination with input mirror substrates with curved front and rear sides. We found that the mode matching for different arm cavity lengths can be nearly completely recovered by changing the size of the

incident laser beam, while the associated change of the eigenmode waist position only degrades the mode matching on the sub-percentage level.

The robustness analysis that was performed shows that the most stringent requirements for manufacturing accuracy are imposed by the curvatures of the input mirror rear surfaces, while deviations from all other design parameters are either mostly uncritical or can easily be compensated for by changing of free parameters.

We have also pointed out that several aspects of the work presented in this paper are of interest for the wider community, such as for instance the possibility of directly measuring coating Brownian noise with the AEI 10 m sub-SQL interferometer at frequencies around 200 Hz. Moreover, the proposed optical layout will allow us to determine how close to the instability one can realistically operate the arm cavities of a Fabry–Perot Michelson interferometer, which is one of the key questions for future GW detectors.

Future work will include the derivation of mirror polishing (and coating) requirements for the marginally stable arm cavities using numerical simulations with mirror maps. In addition to this, we plan to analyze beam jitter requirements as well as laser noise couplings.

Acknowledgments

This work has been supported by the International Max Planck Research School (IMPRS) and the cluster of excellence QUEST (Centre for Quantum Engineering and Space-Time Research). SH and KAS were supported by the Science and Technology Facilities Council (STFC).

References

[1] Goßler S *et al* 2010 *Class. Quantum Grav.* **27** 084023
[2] Westphal T *et al* 2011 *Appl. Phys.* B **106** (3) 551–7
[3] Somiya K *et al* 2009 Conceptual design of an interferometer with sub-SQL sensitivity *LIGO Document Control Center* T0900069
[4] Khalili F Y 2005 *Phys. Lett.* A **334** 67–72
[5] Harry G M *et al* 2002 *Class. Quantum Grav.* **19** 897–917
[6] Kogelnik H and Li T 1966 *Appl. Opt.* **5** 1550
[7] Gretarsson A *et al* 2007 *J. Opt. Soc. Am.* B **24** 2821–8
[8] Arain M A *et al* 2009 Optical layout and parameters for the Advanced LIGO cavities *LIGO Document Control Center* T0900043
[9] Ward R 2010 Advanced Virgo optical design parameters summary *Virgo TDS* VIR-0541B-10
[10] Hild S *et al* 2008 arXiv:0810.0604v2 [gr-qc]
[11] Lück H *et al* 2004 *Class. Quantum Grav.* **21** S985–9
[12] Day R 2011 Central Heating Radius of Curvature Correction System (CHRoCC) used in Virgo *Virgo TDS* VIR-0479A-11
[13] Numata K *et al* 2003 *Phys. Rev. Lett.* **91** 260602
[14] Black E *et al* 2004 *Phys. Lett.* A **328** 1–5
[15] Schnupp L 1988 Presentation given at the *European Collaboration Meeting on Interferometric Detection of Gravitational Waves (Sorrento, Italy)*
[16] Freise A *et al* 2004 *Class. Quantum Grav.* **21** S1067
[17] Drever R W P *et al* 1983 *Appl. Phys.* B **31** 97–105